



OPEN ACCESS

EDITED BY
Emanuela Grassilli,
University of Milano Bicocca, Italy

REVIEWED BY
Haitao Wang,
Center for Cancer Research (NIH),
United States
Ada Hang-Heng Wong,
Independent researcher, Macau,
Macao SAR, China

*CORRESPONDENCE
Wenbo Meng
mengwb@lzu.edu.cn
Yu Liu
yuliu_001@163.com

[†]These authors have contributed
equally to this work and share
first authorship

SPECIALTY SECTION
This article was submitted to
Gastrointestinal Cancers: Hepato
Pancreatic Biliary Cancers,
a section of the journal
Frontiers in Oncology

RECEIVED 30 June 2022
ACCEPTED 31 August 2022
PUBLISHED 16 September 2022

CITATION
Xia Z, Li M, Hu M, Lin Y, Atteh LL,
Fu W, Gao L, Bai M, Huang C, Yue P,
Liu Y and Meng W (2022)
Phosphoproteomics reveals that
cinobufotalin promotes intrahepatic
cholangiocarcinoma cell apoptosis by
activating the ATM/CHK2/p53
signaling pathway.
Front. Oncol. 12:982961.
doi: 10.3389/fonc.2022.982961

COPYRIGHT
© 2022 Xia, Li, Hu, Lin, Atteh, Fu, Gao,
Bai, Huang, Yue, Liu and Meng. This is
an open-access article distributed under
the terms of the [Creative Commons
Attribution License \(CC BY\)](https://creativecommons.org/licenses/by/4.0/). The use,
distribution or reproduction in other
forums is permitted, provided the
original author(s) and the copyright
owner(s) are credited and that the
original publication in this journal is
cited, in accordance with accepted
academic practice. No use,
distribution or reproduction is
permitted which does not comply with
these terms.

Phosphoproteomics reveals that cinobufotalin promotes intrahepatic cholangiocarcinoma cell apoptosis by activating the ATM/CHK2/p53 signaling pathway

Zhili Xia^{1†}, Minzhen Li^{2†}, Meng Hu^{3†}, Yanyan Lin^{4,5},
Lawrence Lower Atteh¹, Wenkang Fu¹, Long Gao¹,
Mingzhen Bai¹, Chongfei Huang¹, Ping Yue^{4,5},
Yu Liu^{3*} and Wenbo Meng^{1,4,5*}

¹The First Clinical Medical College, Lanzhou University, Lanzhou, China,

²Department of Gynecology and Obstetrics, West China Second University Hospital, Sichuan University, Chengdu, China, ³State Key Laboratory of Biotherapy, West China Hospital, Sichuan University, and Collaborative Innovation Center of Biotherapy, Chengdu, China, ⁴The Department of General Surgery, The First Hospital of Lanzhou University, Lanzhou, China, ⁵Gansu Province Institute of Hepatopancreatobiliary Surgery, Lanzhou, China

Intrahepatic cholangiocarcinoma (ICC) is a malignant tumor that originates from bile duct's epithelial cells and is usually characterized by insidious symptoms and poor prognosis. Cinobufotalin (CB), an active ingredient obtained from the Traditional Chinese Medicine ChanSu, is purported to exhibit a wide range of antitumor activities. However, the mechanism by which it achieves such pharmacological effects remains elusive. Here, we disclosed the mechanism of action by which CB inhibits ICC cells. Initial experiments revealed that the proliferation of RBE and HCCC-9810 cells was significantly inhibited by CB with IC50 values of 0.342 μ M and 0.421 μ M respectively. CB induced the expression of caspase-3 subsequently leading to the apoptosis of ICC cells. Phosphoproteomics revealed that the phosphorylation of many proteins associated with DNA damage response increased. Kinase-substrate enrichment analysis revealed that ATM was activated after CB treatment, while CDK1 was inactivated. Activated ATM increased p-CHK2-T68 and p-p53-S15, which promoted the expression of FAS, DR4 and DR5 and triggered cell apoptosis. In summary, this work reveals

the role of CB in inducing DNA damage and cell apoptosis involved in the activation of the ATM/CHK2/p53 signaling pathway, and indicates that CB may serve as a chemotherapeutic drug candidate for ICC treatment.

KEYWORDS

cinobufotalin, phosphoproteome, intrahepatic cholangiocarcinoma, DNA damage, apoptosis, ATM/CHK2/p53 signaling pathway

Introduction

Cholangiocarcinoma may be classified as intrahepatic, perihilar, and distal according to its anatomical location in relation to the biliary tree. Intrahepatic cholangiocarcinoma (ICC), located above the confluence of the left and right hepatic ducts, is a malignant tumor originating from biliary epithelial cells and is characterized by a high degree of malignancy, insidious symptoms, and poor prognosis (1). The incidence of ICC has increased rapidly over the past few decades (2–4), with the highest incidence in Thailand at approximately 0.096% in males (5). The pathogenic factors and pathogenesis of cholangiocarcinoma are still inconclusive. A recent meta-analysis has showed that bile duct cysts, gallstones, liver cirrhosis, and hepatitis B and C viruses are risk factors for intrahepatic and extrahepatic cholangiocarcinoma (6). At present, the main strategies for cholangiocarcinoma treatment are surgical resection and chemotherapy (7). However, current chemotherapy drugs are limited in efficacy and prone to resistance. Patients with locally advanced or metastatic cholangiocarcinoma receiving standard chemotherapy regimens (gemcitabine and cisplatin) have a median overall survival of less than one year (8). Emerging targeted drugs, such as FGFR inhibitors, IDH inhibitors and PD-1 monoclonal antibodies, have become promising (7, 9), but their clinical applications are limited due to the high prices and restricted applicable population. Therefore, it is still urgent to explore new, safe, universal and effective anti-cholangiocarcinoma drugs.

Traditional Chinese Medicine, included some chemotherapeutic compounds, has received increased attention. Cinobufotalin (CB), an active ingredient of the Traditional Chinese Medicine ChanSu, is a bufadienolide derived from toad venom (10). A two-phase solvent system, consisting of hexane/ethyl acetate/methanol/water at 4:6:2:4 V/V, 4:6:2.5:4 V/V and 4:6:3.2:4 V/V, was used to separation and purification of cinobufotalin from ChanSu, based on a high speed counter current chromatography (11). CB is known to have antitumorogenic activities and increase chemosensitivity (12–14). In addition, Cinobufotalin injection is widely used as an adjunctive anti-tumor therapy for lung cancer and hepatocellular carcinoma (15–18). However, the mechanism of action of CB remained elusive.

In this study, we found that CB inhibited ICC cell proliferation and promoted cell apoptosis. By using

phosphoproteomics, we found significant changes in the proteome and phosphorylome associated with DNA damage and apoptosis in response to CB treatment. Further investigations demonstrated that CB induced ICC cell apoptosis by activating the ATM/CHK2/p53 signaling pathway and upregulating the expression of FAS, DR4 and DR5. Our results collectively indicate that CB may serve as a potential anti-cholangiocarcinoma drug.

Methods

Cell culture

The human ICC cell lines (RBE and HCCC-9810) were purchased from the National Biomedical Experimental Cell Resource Bank of China (Beijing, China). CB was purchased from Biopurify Phytochemicals Ltd (Chengdu, China). The ICC cells were grown in RPMI 1640 medium (#10270-106, Gibco) containing 10% (v/v) fetal bovine serum (#SFBE, NATOCOR), 100 U/mL penicillin and 100 µg/mL streptomycin (#15140-122, Gibco) and placed in an incubator with a constant temperature of 37°C and 5% CO₂.

Cell proliferation and colony formation assays

Cell proliferation ability was measured by the cell counting kit-8 (CCK-8). Cells were seeded in 96-well plates at a density of 3.5×10^3 cells/well. After overnight incubation, the cells were treated with different concentrations of CB (0, 0.1, 0.25, 0.5, 1.0 and 2.0 µM) for 24 h, 48 h, and 72 h. Ten microliters of CCK-8 (Yeasen Biotechnology, Shanghai, China) was added, and the optical density (OD) value was detected at a wavelength of 450 nm after incubation at 37°C for 2 h. In the colony formation experiment, cells were seeded in 6-well plates for 2000 cells/well. Cells were treated with CB after sticking to the plates for 24 h, and the experiment was terminated after 2 weeks of culture. Clones were fixed with 4% paraformaldehyde for 30 minutes and stained with crystal violet for another 30 minutes.

Apoptosis analysis by flow cytometry

Cells were treated with different concentrations of CB (0, 0.25 and 0.5 μM) for 48 h. According to the operating instructions, cells were harvested and washed twice with pre-cooled PBS, and stained with Annexin V-PE and 7-AAD solutions (Vazyme Biotech Co, Nanjing, China) at 25°C for 10 min in the dark. BD FACSCelesta™ multicolor flow cytometer (BD Bioscience, Franklin Lakes, NJ, USA) was used for detection. Annexin V-PE positive/7-AAD negative indicates early apoptotic cells, and Annexin V-PE positive/7-AAD positive means late apoptotic cells. All the above data were statistically analyzed in SPSS 20 (IBM, Chicago, IL, USA). Student's *t*-test was used to compare two groups, and ANOVA was used for multiple groups. GraphPad Prism 8.0 (GraphPad, San Diego, CA, USA) was used for graphing.

Protein extraction and TMT labeling

RBE cells treated with different concentrations (0, 0.25 μM) of CB for 48 h were harvested, washed twice with pre-cooled PBS, lysed in RIPA buffer (150 mM NaCl, 50 mM Tris (pH = 7.5), 1% NP-40 (v/v), 0.5% sodium deoxycholate (w/v)), 1×protease inhibitors, 1× phosphatase inhibitors), and sonicated with JY92-IIN sonicator (NingBoXinYi, Ningbo, China) for 3 min (parameters: on for 3 s, off for 10 s, power 30%). The protein extracts were centrifuged at 16000 g for 30 minutes. The protein concentration was determined with a BCA kit (Beyotime Biotech, Shanghai, China). One hundred micrograms of proteins from each sample were reduced with Tris (2-carboxyethyl) phosphine (TCEP) at a final concentration of 10 mM for 1 hour at 56°C, and alkylated with iodoacetamide at 20 mM in the dark. The proteins were then precipitated with methanol, chloroform and water ($\text{CH}_3\text{OH} : \text{CHCl}_3 : \text{H}_2\text{O} = 4:1:3$) and digested with trypsin (1:50, w/w, trypsin/protein) overnight at 37°C. The peptides of each sample were labeled with TMT (Thermo Fisher Scientific, Waltham, MA, USA) reagent according to the specification. After quenching with 5% hydroxylamine, the TMT-labeled peptides were mixed, and concentrated to dryness.

Peptide fractionation

TMT-labeled peptides were desalted and then fractionated using reversed-phase high-performance liquid chromatography (RP-HPLC, SHIMADZU-LC-2030 Plus) under basic conditions. The mobile phase was composed of buffer A (ACN 98%, H₂O 2%, pH = 10) and buffer B (90% ACN, H₂O 10%, pH = 10). A standard 120 min LC gradient was used as follows: 0-2 min, 2% Buffer B; 2-60 min, 2-35% Buffer B; 60-95 min, 35-55% Buffer B; 95 -105 min, 55-90% Buffer B; 105~120 min, 90~2% Buffer B,

and the flow rate was 1 ml/min. The mixture was separated into 120 fractions and combined into 20 parts. Then the samples were analyzed by mass spectrometry after desalting. For phosphorylomics, C18 solid-phase extraction cartridge (100 mg packing material) was used to divide the mixture into 18 fractions, which were finally combined into 6 parts and desalted.

Enrichment of phosphopeptides

Twenty microliters of Fe-NTA agarose beads were used for the enrichment of phosphopeptides for each sample. The agarose beads were washed with 1 mL of washing buffer (80% ACN%, 0.1% TFA) 3 times and then transferred into six 1.5 mL EP tubes. Desalting peptides were resuspended in 300 μL washing buffer, and incubated with Fe-NTA agarose beads at room temperature for 45 minutes on a 3D shaker. Then the beads were washed with washing buffer 5 times and eluted with 150 μL elution buffer (50% ACN, 2.5% ammonia). The solution was neutralized with 8 μL 20%TFA, concentrated to dryness, and analyzed by mass spectrometry after desalting.

Mass spectrometry analysis

Desalted peptides were resuspended in buffer A (2% ACN, 0.1% FA) and further analyzed by EASY-nanoLC 1000 coupled to a high-resolution mass spectrometer (Q Exactive Plus, Thermo Fisher Scientific). The samples were loaded onto a 75 μm (inner diameter) \times 2 cm (length) trap column and a 75 μm (inner diameter) \times 15 cm (length) analytical column, which were packed with C18 particles (DIKMA) in-house. Data-dependent acquisition (DDA) was performed in positive ion mode, and samples were analyzed with a 105 min or 65 min gradient from 12 or 13 to 100% buffer B (80% ACN, 0.1% FA) for proteomics and phosphoproteomics, respectively, at a flow rate of 330 nL/min. The full-scan MS spectrum ranged from 350 to 1600 m/z with a resolution of 70,000 at m/z = 200. The automatic gain control (AGC) value was set to $3e^6$, and the maximum injection time was 20 ms. In the MS/MS scan, the top 15 most abundant precursor ions were selected with an isolation window of 0.6 m/z. For the proteome, the collision energy (NCE) was set to 30%, but the phosphopeptides were fragmented with gradient energies of 25% and 31% NCE. The AGC value for MS/MS was set to $1e^5$, the maximum injection time was 100 ms, and the resolution was 35,000. Precursor ions with charge state $z = 1, 7-8$ or unassigned were excluded.

Database search

The raw mass spectrometry files of the 20 fractions of the proteome and the 6 fractions of the phosphorylome were

searched using Maxquant (version 1.6.2.3), referring to the Swiss-Prot human protein sequence database (20413 sequence, 2019/02/13 update), separately. The mass deviation of precursor ions was set to within 10 ppm, and the mass deviation of fragment ions was 0.02 Da. The maximum number of missing cleavage sites was 2. Cysteine carbamidomethylation and methionine oxidation were fixed modifications. For the phosphorylome, phosphorylation (S/T/Y) was set as a dynamic modification. The false discovery rate of peptides and proteins was less than 1%. The minimum number of amino acids in a peptide is 6, and the maximum molecular weight of a peptide is 12,000 Da.

Proteome data processing

After removing reverse and contaminant proteins, the total protein intensities of all samples were normalized, and proteins with unique peptides ≥ 2 were used for subsequent data analysis. The phosphosites with localization probabilities greater than 0.75 were retained. Proteins and phosphosites with $p < 0.05$ (Student's *t*-test) and ratio (CB/Ctr) > 1.25 or < 0.8 were defined as significantly changed after CB treatment. The algorithm for summarizing the change in total phosphorylation (ΔP) at different sites on the same protein is as follows: the ΔP s value of each phosphoprotein is equal to the "sum of \log_2 (fold change)" of all significantly changed phosphopeptides of protein isoforms encoded by the same gene (19).

Bioinformatics

Kyoto Encyclopedia of Genes and Genomes (KEGG) enrichment analysis of significantly differentially expressed proteins was performed by DAVID 6.8 (<https://david.ncicrf.gov/home.jsp>) (20, 21). Gene function enrichment and molecular network interaction analysis of differentially phosphorylated proteins were carried out by Metascape (<https://metascape.org>) (22). Combined analysis of quantified proteomic and phosphoproteomic data with literature-based proteome-wide signaling networks was based on the SIGNaling Network Open Resource 2.0 Database (SIGNOR 2.0) (<https://signor.uniroma2.it>) (23). Data processing and visualization were performed using the following R packages: ComplexHeatmap, ggplot2, ggpubr, ggthemes, dplyr, ggExtra, and readxl.

Immunoblotting

Cells were treated with CB (0, 0.25, 0.5 μM) for 48 h and then the cell lysates were analyzed by immunoblotting. The primary antibodies used in this study were as follows: ATM

antibody (ET1606-20, Huabio), phospho-ATM-S1981 antibody (ET1705-50, Huabio), phospho-AKT-S473 antibody (4060S, Cell Signaling Technology), AKT antibody (4685S, Cell Signaling Technology), phospho-mTOR-S2448 antibody (5536T, Cell Signaling Technology), mTOR antibody (2983T, Cell Signaling Technology), phospho-p70S6K-T389 antibody (9234S, Cell Signaling Technology), p70S6K antibody (9202S, Cell Signaling Technology), Bcl-2 antibody (ET1702-53, Huabio), active+pro Caspase-3 antibody (ET1608-64, Huabio), active Caspase-3 antibody (ET1602-47, Huabio), p53 antibody (ab26, Abcam), γH2AX antibody (201082-2A9, ZEN-BIOSCIENCE), phospho-p53-S15 antibody (YP0205, ImmunoWay), CHK2 antibody (ET1610-52, Huabio), phospho-CHK2-T68 antibody (29012-1-AP, Proteintech) and GAPDH antibody (60004-1-Ig, Proteintech). The relative protein intensity was calculated by ImageJ software.

Results

CB inhibits ICC cell proliferation and promotes apoptosis

The chemical structure of CB is shown in Figure 1A. CB significantly inhibited the proliferation of ICC cells, including RBE and HCCC-9810 cells. The IC₅₀ values of CB in RBE and HCCC-9810 cells were 0.342 μM and 0.421 μM , respectively (Figures 1B, C). Meanwhile, we found that application of 0.5 μM cinobufotalin in RBE cells shows higher cell viability at 72 h than 48 h post-treatment (Figure 1B), which may be related to the cell contact inhibition over longer periods of treatment in the untreated group for the too high cell density. Therefore, the calculated relative cell viability may be slightly higher at the timepoint of 72 h than at 48 h. In addition, CB also significantly inhibited the colony formation of ICC cells (Figures 1D–G). Flow cytometry analysis revealed dramatically increased numbers of early and late apoptotic RBE and HCCC-9810 cells as the concentrations of CB increased (Figures 1H, I). Consistently, immunoblotting showed that the cleaved caspase-3, an apoptosis-associated protein marker, was up-regulated in both ICC cell lines, and the oncoprotein Bcl-2 was down-regulated in RBE cells after CB treatment (24–26) (Figure 1J). Collectively, the above results indicate that CB can inhibit ICC cell proliferation and induce cell apoptosis.

Phosphoproteomics reveals CB-regulated signaling pathway

To profile the CB-induced molecular changes in ICC cells, we performed comparative proteomic and phosphoproteomic analyses between CB-treated and untreated RBE cells with 3 biological replicates (Figure 2A). A total of 6740 proteins were

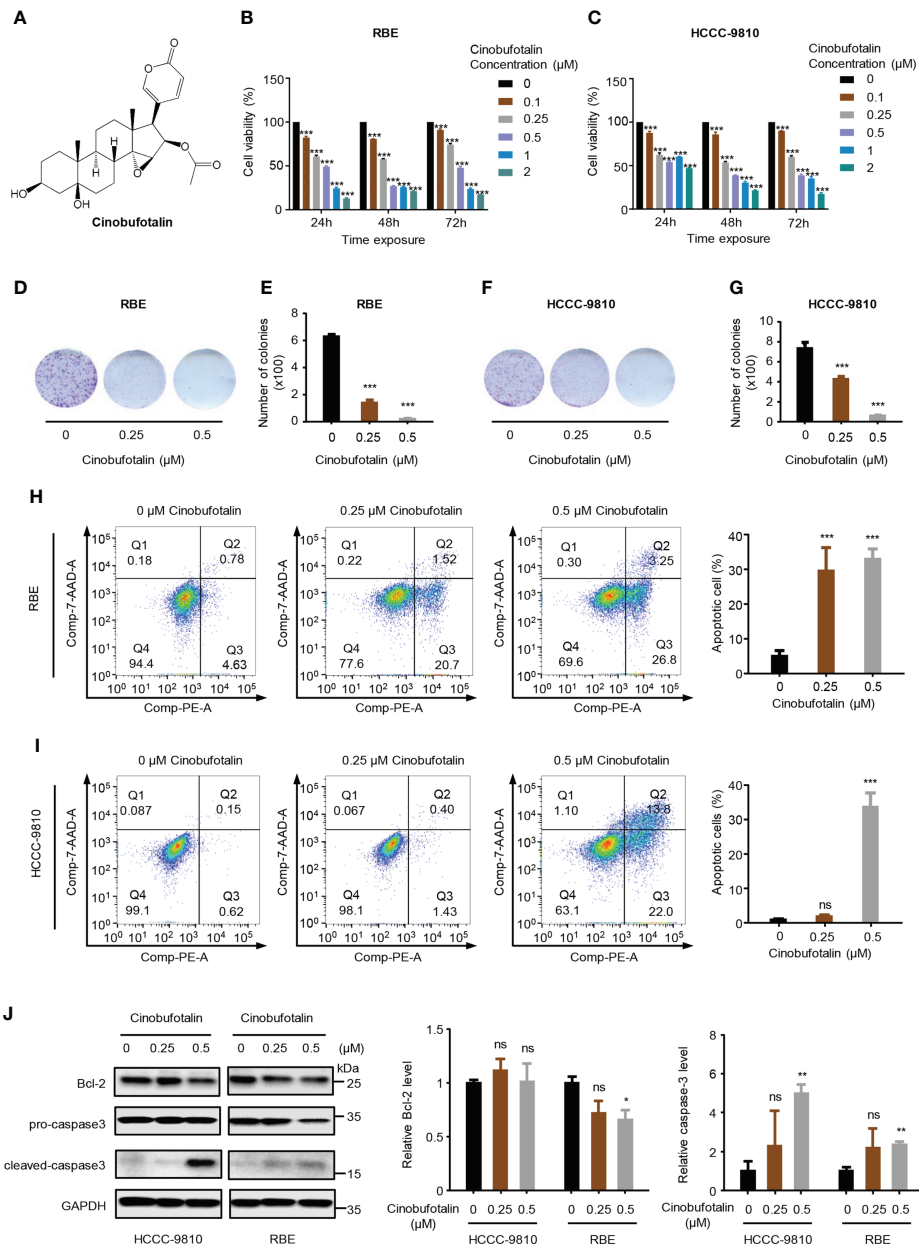
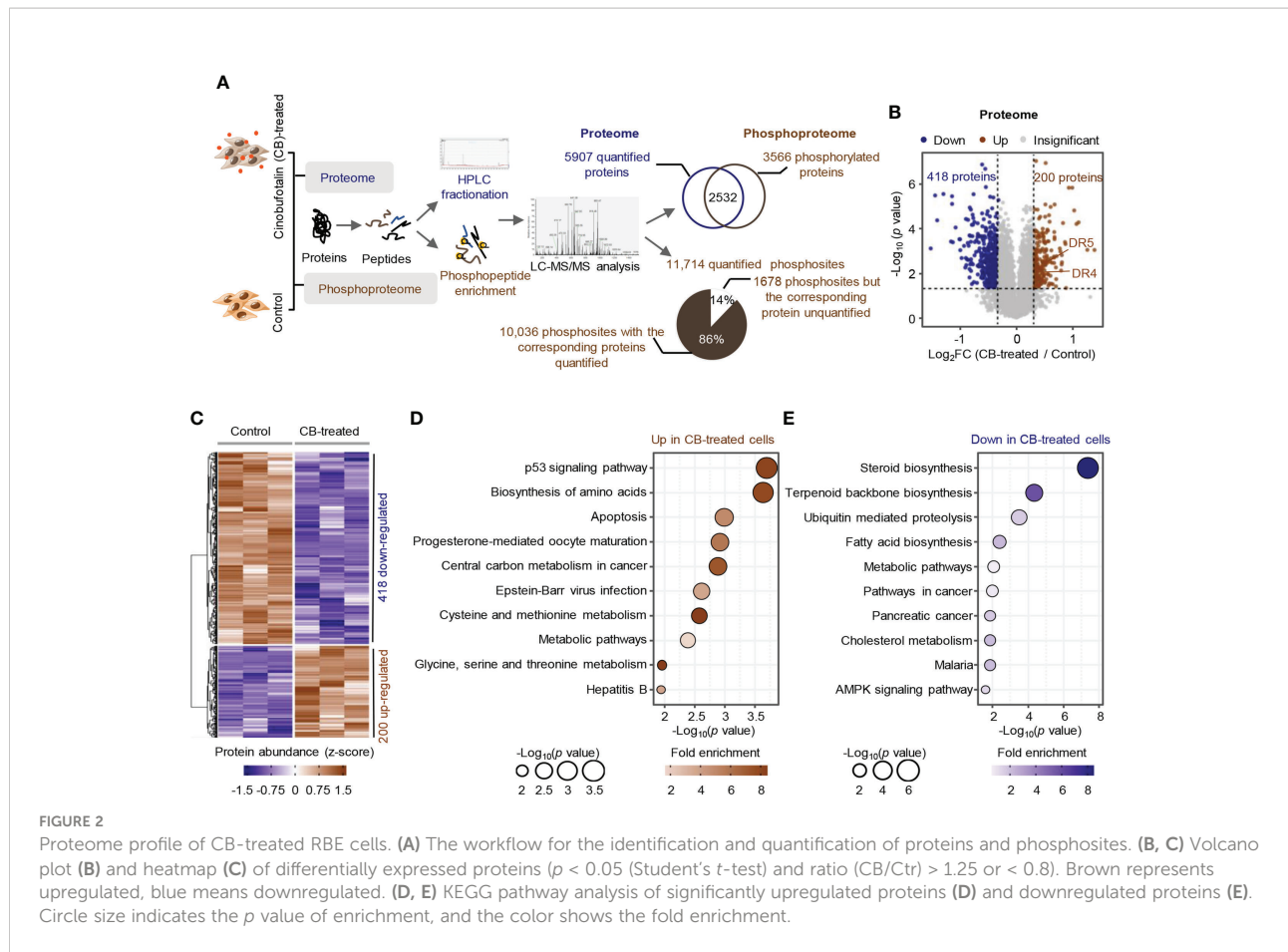


FIGURE 1
 Cinobufotalin inhibits ICC cell proliferation and promotes cell apoptosis. **(A)** Chemical structure of cinobufotalin (CB). **(B, C)** RBE and HCCC-9810 cells were treated with 0, 0.1, 0.25, 0.5, 1.0 and 2.0 μM of CB, respectively, for 24 h, 48h and 72h, and cell viability was measured by Cell counting kit-8 (CCK-8) assay. **(D–G)** Colony formation **(D, F)** and the statistics of colony counts **(E, G)** of RBE and HCCC-9810 cells. **(H–I)** Flow cytometry analysis of cell apoptosis by Annexin V-PE/7-AAD staining. **(J)** The expression of apoptosis-related proteins in RBE and HCCC-9810 cells measured by immunoblotting and calculated by ImageJ software. * $p < 0.05$, ** $p < 0.01$, *** $p < 0.001$, ns denotes statistically insignificant difference, Student's *t*-test.

identified by proteomics, and 5907 were quantified with unique peptides ≥ 2 (Supplemental Table S1). Among them, 200 proteins were significantly up-regulated after CB treatment (ratio (CB/Ctr) > 1.25 , $p < 0.05$), and 418 proteins were significantly down-regulated (ratio (CB/Ctr) < 0.8 , $p < 0.05$)

(Figure 2B and Supplemental Table S2). Among the up-regulated proteins, DR4 (also known as TNFRSF10A and TRAIL-R1) and DR5 (also known as TNFRSF10B and TRAIL-R2) are the two main types of tumor necrosis factor-related apoptosis-inducing ligand (TRAIL) receptors in humans and



can induce cell apoptosis (27, 28) (Figures 2B, C). For example, in Hep3B hepatoma cells, morin up-regulates DR4 and DR5, and activates caspase-3, -8, and -9 to promote tumor cell apoptosis (29). In addition, DNA damage can induce the expression of DR5 through a p53-dependent pathway, which further promotes tumor cell apoptosis (30). KEGG enrichment analysis showed that the up-regulated proteins were mainly associated with p53, biosynthesis of amino acids and apoptosis signaling pathways and amino acid metabolism, such as cysteine and methionine metabolism and glycine, serine and threonine metabolism (Figure 2D). The down-regulated proteins were involved in steroid biosynthesis, terpenoid biosynthesis, ubiquitin mediated proteolysis, fatty acid biosynthesis and cholesterol metabolism, as well as the AMPK signaling pathway and tumor-related signaling pathway (Figure 2E).

Phosphorylomics identified a total of 16,445 phosphosites, of which 11,714 were quantified with phosphorylation localization probability greater than 0.75. Of the 11,714 quantified phosphosites, the corresponding proteins of 10,036 phosphosites were quantified as well and were used for the subsequent analysis (Figure 3A). Consistent with previous mass spectrometry-based analyses (31, 32), the identified

phosphorylation events in ICC cells mainly occurred on serine residues (87.4%) (Figure 3B) and most proteins had fewer than 3 identified phosphosites (Figure 3C). The changes of the 10036 phosphosites between CB-treated and untreated RBE cells were calculated and normalized to protein intensities (Supplement Table S3). As a result, 321 up-regulated phosphosites (ratio (CB/Ctr) > 1.25 , $p < 0.05$) and 1541 down-regulated phosphosites (ratio (CB/Ctr) < 0.8 , $p < 0.05$) were obtained (Figure 3D and Supplement Table S4). Although the signaling pathways including signaling by Rho GTPases, Miro GTPases and RHOTB3 were enriched using proteins with up- or down-regulated phosphosites (Figures 3E, F), we still observed many differences between them. For example, pathways such as cellular response to DNA damage stimulus and regulation of cellular localization were enriched using proteins with up-regulated phosphosites (Figure 3E), while metabolism of RNA and cell cycle were enriched using proteins with down-regulated phosphosites (Figure 3F).

Further analysis showed that 176 significantly differential phosphosites on 84 proteins were associated with DNA damage. Some well-known DNA damage-related phosphosites, such as NBN-S343/397, MCM3-S681 and MYC-S62 were significantly

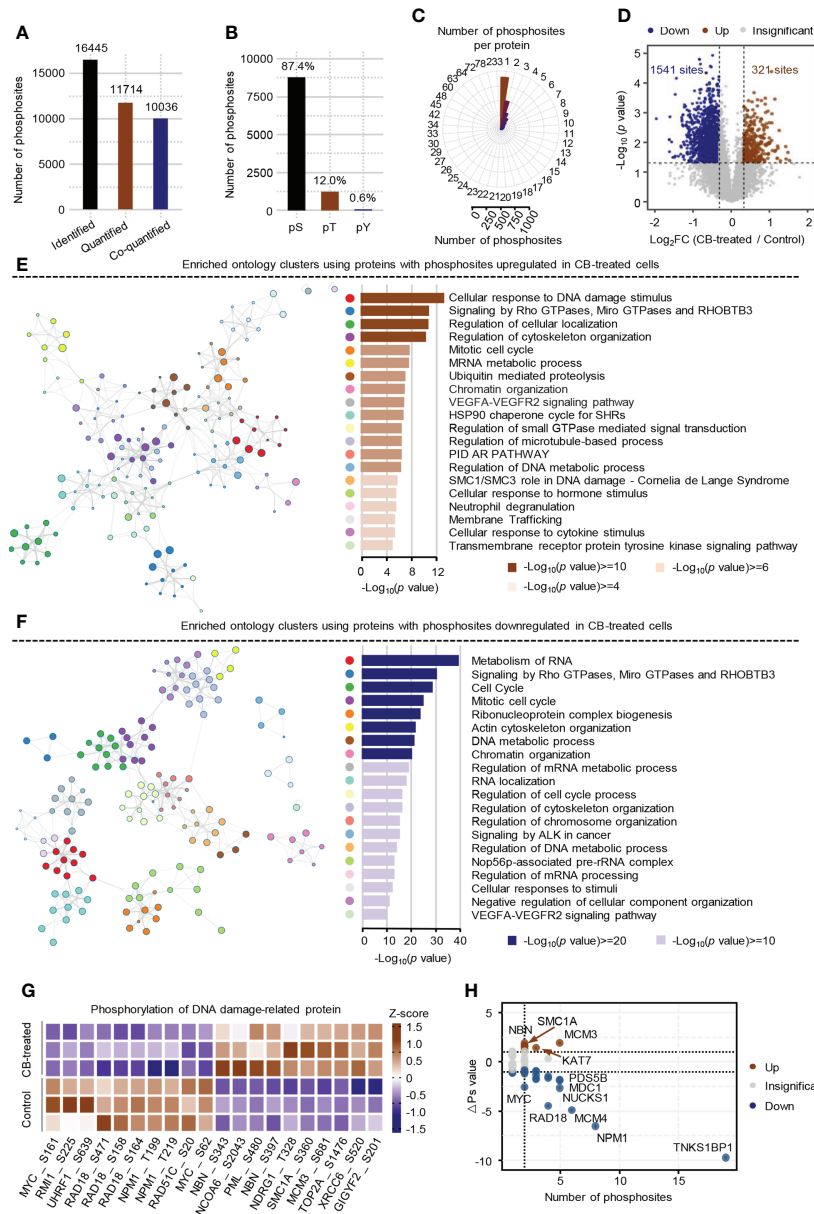


FIGURE 3
 Phosphoproteome profile of CB-treated RBE cells. **(A)** The statistics of identified and quantified phosphosites. Co-quantified means both phosphosites and the corresponding proteins were quantified. **(B)** The percentages of phosphosites on serine, threonine and tyrosine residues. **(C)** The statistics of the number of phosphosites on each protein. **(D)** Volcano Plot of significantly altered phosphosites ($p < 0.05$ (Student's t -test) and ratio (CB/Ctr) > 1.25 or < 0.8). Brown represents up-regulated, blue means down-regulated. **(E, F)** Pathway enrichment analysis of proteins with up-regulated **(E)** and down-regulated **(F)** phosphosites using Metascape. The colors of the dots in the network represents different biological pathways. **(G)** Heatmap of the top 10 DNA damage-related phosphosites using Metascape that were significantly changed in CB-treated versus untreated cells. **(H)** Global ΔP_s analysis of phosphoproteins involved in DNA damage. Brown represents up-regulated, blue means down-regulated.

changed after CB treatment (Figure 3G) (33–36). To obtain the DNA damage associated proteins with the greatest changes in total phosphorylation, we summed the phosphorylation alteration for each protein based on a known algorithm (Supplement Table S5) (19). The results showed that the total

phosphorylation levels of NBN, MCM3, SMC1A and KAT7 were significantly increased, while those of TNKS1BP1, NPM1, MCM4, RAD18, NUCKS1, MYC and many other proteins were significantly decreased (Figure 3H). Collectively, CB may inhibit cell proliferation by inducing DNA damage and apoptosis.

Kinase-substrate enrichment analysis reveals the activation of ATM by CB

We further used the PhosphoSitePlus database in the KSEA APP website to perform a kinase-substrate enrichment analysis based on the 10,036 phosphosites (37, 38), with an FDR cutoff of 0.05 and a substrate count cutoff of 5, and found that ATM kinase substrate motifs, as well as the substrate motifs of other kinases, such as AKT1, ATR, SGK1 and MAPKAPK2, were significantly enriched (Figure 4A), with the phosphorylation levels of ATM, AKT1, ATR, SGK1 and MAPKAPK2 substrates increased after CB treatment (Figure 4B). In addition, we found that the substrate motifs of cell cycle-related kinases such as CDK1/2/5 were also enriched (Figure 4A), and the phosphorylation levels of CDK1/2/5 substrates decreased after CB treatment (Figure 4B).

To further explore intracellular changes in signaling networks after CB treatment, we performed integrative analysis of the proteome and phosphoproteome data using the SIGNOR 2.0 database (23, 32, 39). The results showed that the

downstream substrates of ATM were hyperphosphorylated in RBE cells after CB treatment, while CDK1 and CDK2 substrates were significantly dephosphorylated (Figure 4C). ATM is activated with increased phosphorylation at S1981 and acetylation at K3106 and then initiates the signaling cascade in response to DNA damage (40, 41). Although phosphorylation of ATM at S1981 was not detected in our phosphoproteomic data, we speculated that CB might activate ATM based on the activation of its numerous downstream substrates.

CB promotes apoptosis by activating the ATM/CHK2/p53 signaling pathway

In the above studies, we found that CB induced significant up-regulation of key proteins involved in the p53 and apoptosis signaling pathways in RBE cells (Figure 5A). The phosphorylation levels of ATM substrates, including NBN-S343/397, SMC1A-S957 and BRCA1-S1524, were up-regulated (Figure 5B), while the phosphorylation levels of CDK1

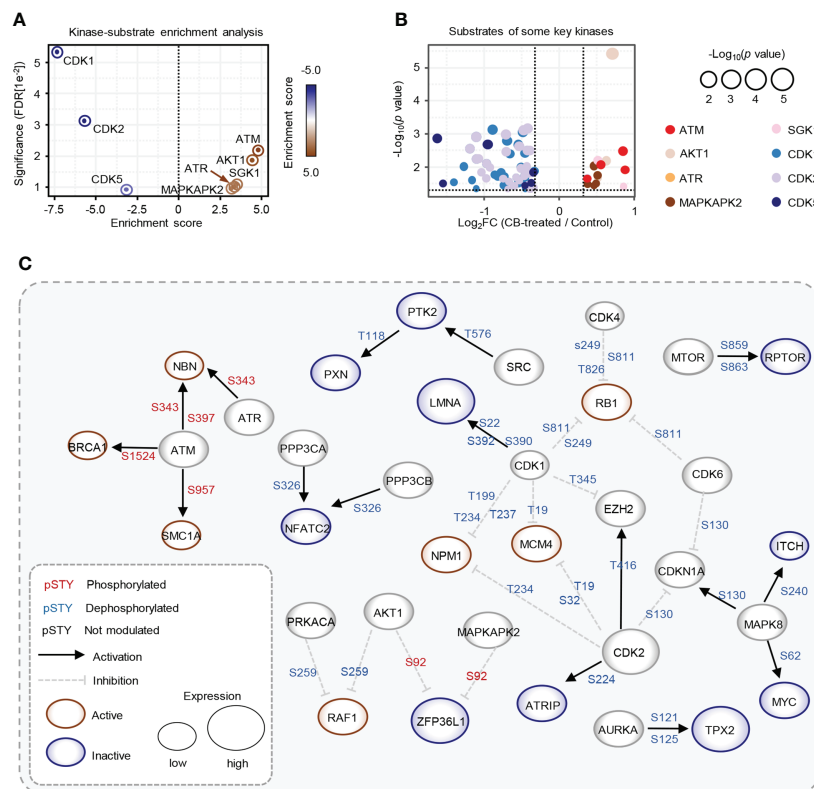


FIGURE 4 Key kinases involved in CB treatment of RBE cells. **(A)** Evaluation of kinase activities by KSEA in CB-treated RBE cells. **(B)** Scatter plot of the significantly changed substrates of key kinases. The color represents different substrates that showed in Figure 4A. **(C)** The phosphoproteome alterations in response to CB treatment were mapped to a literature derived signal network using the SIGNOR 2.0 database. The node size is proportional to the level of protein expression. Blue and red nodes mean inactivated and activated, respectively. Phosphorylation and dephosphorylation reactions on specific residues are represented by edges between nodes.

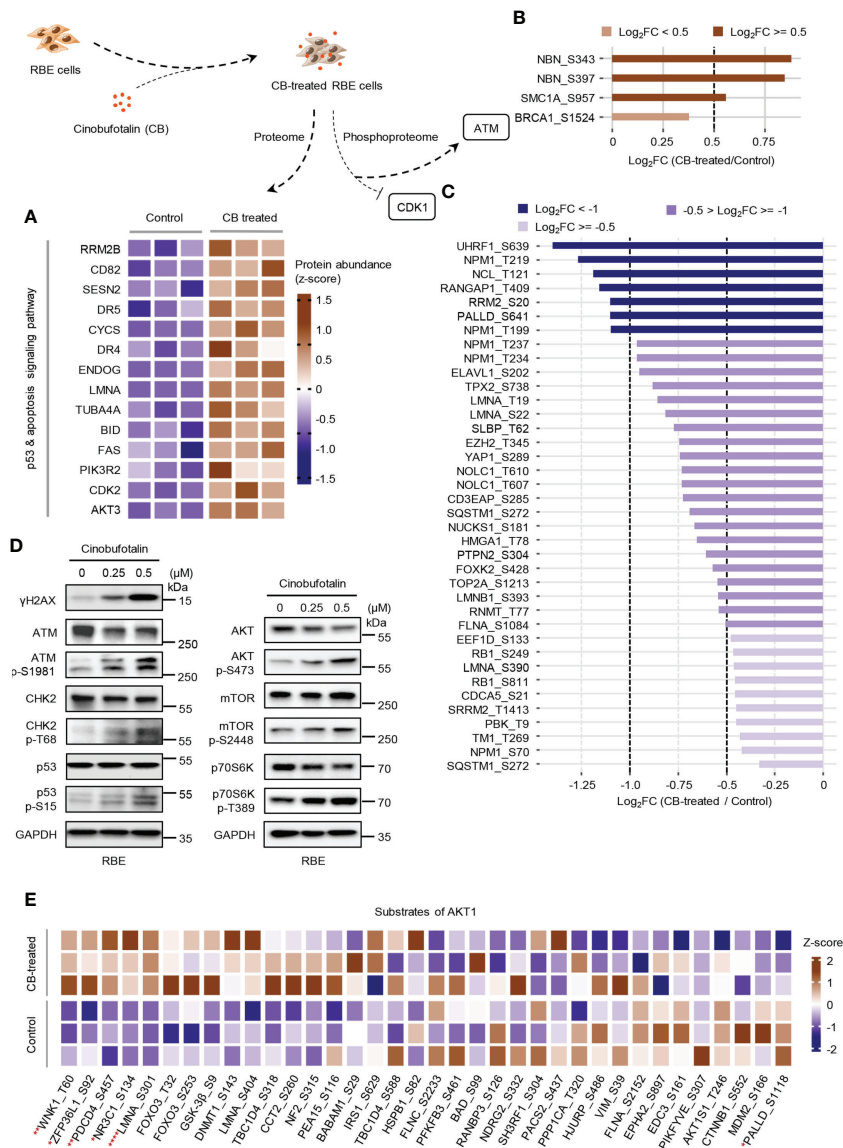


FIGURE 5 CB treatment remodels proteome and phosphoproteome of RBE cells. **(A)** Heatmap of significantly changed proteins of the p53 and apoptosis signaling pathway in CB-treated RBE cells. Brown represents up-regulated, blue means down-regulated. **(B, C)** The statistics of the phosphosites regulated by ATM **(B)** and CDK1 **(C)**. **(D)** Verification of the expression of DNA damage, p53 signaling and AKT signaling pathway-related proteins and phosphosites by immunoblotting. **(E)** The heatmap shows the MS detected phosphosites regulated by AKT1. **p* < 0.05, ***p* < 0.01, *****p* < 0.0001, Student's *t*-test.

substrates, such as UHRF1-S639, NPM1-T219 and NCL-T121, were reduced (Figure 5C). Activated ATM can stimulate CHK2 by promoting phosphorylation at CHK2-T68, which stabilizes and activates p53 by promoting phosphorylation at p53-S15/S20 (42–44). When p53 is activated, cell apoptosis can be induced by up-regulating the FAS, DR4 and DR5 signaling pathways (45–49). Notably, our proteomic data showed that FAS, DR4 and DR5 were up-regulated after CB treatment (Figure 5A). Moreover, the levels of γH2AX, p-ATM-S1981, p-CHK2-T68,

and p-p53-S15 were also significantly increased in CB-treated cells (Figure 5D). Previous studies have demonstrated that the activation of the ATM/CHK2/p53 signaling pathway can inhibit tumor cell growth by inducing apoptosis and cell cycle arrest (42, 50–54). In addition, we found that AKT1 was also activated after CB treatment. In order to further show the changes of AKT1-associated signaling pathways, we summarized AKT1 substrates (Figure 5E). Although some downstream substrates of AKT1 such as FOXO3 and GSK3β showed increased phosphorylation

levels, but the changes were not significant. To further demonstrate our results, we performed Western blotting analysis of AKT1 phosphorylation and its downstream mTOR signaling (AKT Ser473, mTOR S2448 and p70S6K T389), and found that the phosphorylation level of both sites increased, indicating the activation of AKT/mTOR/p70S6K signaling pathway, which might activate pro-survival AKT signaling after DNA damage (Figure 5D) (55). However, the tumor cells underwent apoptosis after CB treatment due to the predominant activation of the ATM/CHK2/p53 apoptotic pathway. Therefore, this work confirms that CB induces DNA damage, activates the ATM/CHK2/p53 signaling pathway and promotes the expression of FAS, DR4 and DR5, thereby promoting apoptosis in ICC cells and ultimately inhibiting cell proliferation (Figure 6).

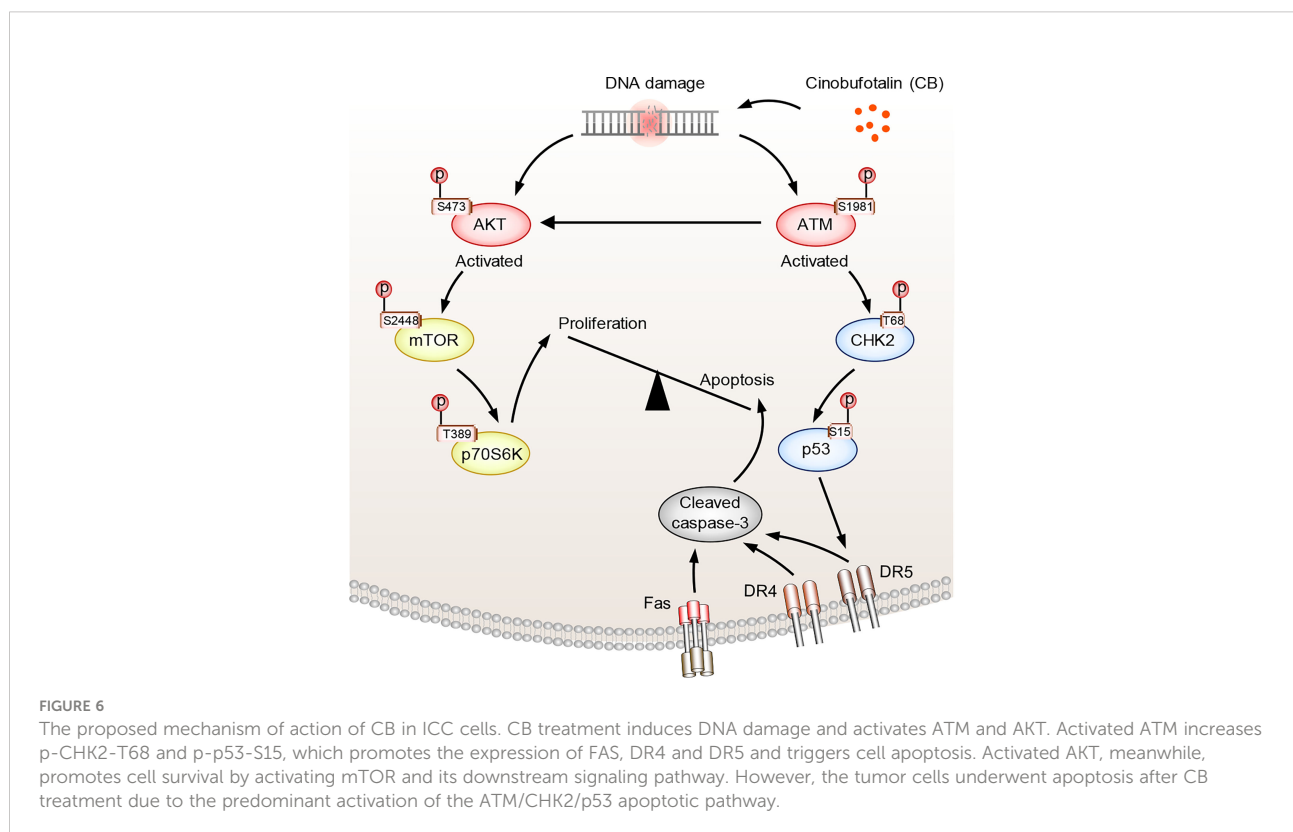
Discussion

As a potential anti-cancer drug, some mechanisms of action of CB have been proposed by previous studies. For example, CB inhibits cancer cell stemness and EMT signaling by regulating the PI3K/AKT/MYC/p53/miR-133a-3p signaling axis (56). It can induce reactive oxygen species (ROS) production and FAS up-regulation, which in turn leads to DNA damage and caspase-dependent apoptosis (12, 13). However, a comprehensive understanding of the mechanisms by which CB induces DNA

damage, apoptosis and cell cycle arrest is still lacking. This study revealed that CB inhibits ICC cell proliferation through the ATM/CHK2/p53 signaling pathway, providing a new perspective for understanding the anti-tumor mechanism of CB.

The MRN complex (MRE11/RAD50/NBN) is a DNA double-strand break sensor in eukaryotes involved in the early steps of DNA double-strand break sensing and repair, DNA excision, activation of DNA damage checkpoints, activation of cell cycle checkpoints, chromatin remodeling, and recruitment of DNA repair factors (57–59). NBN (NBS1) is a component of the MRN complex and has many serine residues that can be phosphorylated. Among them, S343, S397 and S615 can be phosphorylated by ATM, and ATM-mediated phosphorylation of NBN is essential for the DNA damage response (34). In addition, radiation-induced DNA damage can lead to increased phosphorylation levels of MCM3 at S681/S728/S734 (35). Consistently, our results showed that CB treatment of RBE cells leads to DNA damage and up-regulation of phosphorylation at both NBN-S343/397 and MCM3-S681, confirming the role of CB in inducing DNA damage.

We also observed significant dephosphorylation events at S62 and S161 of MYC in our phosphoproteomics analysis after CB treatment. As a classic oncogenic factor, MYC, a downstream regulator of the PI3K/AKT signaling pathway, can negatively regulate p53 (56, 60). Dephosphorylation of MYC at S62 can lead to decreased MYC activity and protein stability, thereby



inhibiting cell proliferation (36, 61). Therefore, we assume that MYC may serve as an effector molecule to promote the function of CB in inhibiting ICC cell proliferation.

TNKS1BP1 is a member of the poly ADP ribose polymerase (PARP) superfamily protein associated with DNA damage repair. Overexpression of TNKS1BP1 induces autophosphorylation of DNA-PKcs at S2056, thereby increasing DNA damage repair ability (62). In this study, we found that the phosphorylation level of TNKS1BP1 was significantly decreased after CB treatment, which may be associated with CB induced DNA damage. Moreover, ubiquitination is an important post-translational modification of proteins, which plays a crucial role in maintaining cell function (63). We also noticed that dephosphorylation events occurred on some serine residues of E3 ligases, such as RAD18 at S158/S164/S471 and RAD51C at S20 after CB treatment. RAD18 and RAD51 are DNA damage repair factors and participate in DNA damage repair (64–66). The roles of phosphorylation of RAD18 and RAD51 in DNA damage repair are less understood and worthy of further exploration.

Although the mechanism of CB has been disclosed, this study also had some limitations. First, the function of CB in inhibiting cancer cell proliferation needs to be verified in animal models, and the effects of CB on normal organs require a comprehensive evaluation. Second, the direct cellular targets of CB are still unknown. CB has an epoxy group, which may react with some nucleophilic groups in proteins and other biological macromolecules and initiate the DNA damage process. In addition, CB is a cardiotonic steroids or bufadienolides. The structure of CB is very close to that of cholesterol and other steroid derivatives. According to the pathway enrichment result, we assume that cinobufotalin may competitively bind to the receptor of these steroids and affect the steroid biosynthesis. However, this assumption needs to be verified with more experiments.

Conclusion

Collectively, in this study, we investigated the function of CB in ICC cells by performing phosphoproteomics. Several findings were made. First, proteomic analysis showed that the p53 and apoptosis signaling pathways were activated after CB treatment. The proteins in these signaling pathways, such as DR4, DR5, FAS, CYCS, ENDOG, RRM2B, TUBA4A and SESN2, were significantly up-regulated, and the changes in some classical markers among them were further verified. Second, phosphoproteomics revealed the activation of some DNA damage-associated kinases after CB treatment, such as ATM, AKT1 and ATR, while the cell cycle-related kinases CDK1/2/5 were inactivated. Finally, we demonstrated that CB promoted apoptosis in ICC cells and inhibited cell proliferation by activating the DNA damage associated ATM/CHK2/p53 signaling pathway and promoting the expression of FAS, DR4 and DR5. In summary, this work preliminarily reveals

the mechanism of action of CB and provides a potential chemotherapeutic drug candidate for cholangiocarcinoma treatment.

Data availability statement

The datasets presented in this study can be found in online repositories. The names of the repository/repositories and accession number(s) can be found in the article/Supplementary Material.

Author contributions

WM and YL designed the experiment; ZX, ML, and MH handled the sample preparation and data analysis; ZX drafted and revised the manuscript; the remaining authors provided technical support and suggestions. All authors have approved the final version of the manuscript.

Funding

This work was supported by Grant(s) from the National Natural Science Foundation of China (82060551 to WM), the Health Industry Scientific Research Program of Gansu Province (GSWSKY2020-11 to YYL), the Lanzhou Cheng guan District Science and Technology Plan Project (2019JSCX0092 to YYL) and the Key Talent Program of Gansu Province (2019RCXM077 to WM).

Conflict of interest

The authors declare that the research was conducted in the absence of any commercial or financial relationships that could be construed as a potential conflict of interest.

Publisher's note

All claims expressed in this article are solely those of the authors and do not necessarily represent those of their affiliated organizations, or those of the publisher, the editors and the reviewers. Any product that may be evaluated in this article, or claim that may be made by its manufacturer, is not guaranteed or endorsed by the publisher.

Supplementary material

The Supplementary Material for this article can be found online at: <https://www.frontiersin.org/articles/10.3389/fonc.2022.982961/full#supplementary-material>

References

- Razumilava N, Gores GJ. Cholangiocarcinoma. *Lancet* (2014) 383(9935):2168–79. doi: 10.1016/S0140-6736(13)61903-0
- Kelley RK, Bridgewater J, Gores GJ, Zhu AX. Systemic therapies for intrahepatic cholangiocarcinoma. *J Hepatol* (2020) 72(2):353–63. doi: 10.1016/j.jhep.2019.10.009
- Zhang H, Yang T, Wu M, Shen F. Intrahepatic cholangiocarcinoma: Epidemiology, risk factors, diagnosis and surgical management. *Cancer Lett* (2016) 379(2):198–205. doi: 10.1016/j.canlet.2015.09.008
- Bridgewater J, Galle PR, Khan SA, Llovet JM, Park JW, Patel T, et al. Guidelines for the diagnosis and management of intrahepatic cholangiocarcinoma. *J Hepatol* (2014) 60(6):1268–89. doi: 10.1016/j.jhep.2014.01.021
- Khan SA, Toledano MB, Taylor-Robinson SD. Epidemiology, risk factors, and pathogenesis of cholangiocarcinoma. *HPB (Oxford)* (2008) 10(2):77–82. doi: 10.1080/13651820801992641
- Clements O, Eliahoo J, Kim JU, Taylor-Robinson SD, Khan SA. Risk factors for intrahepatic and extrahepatic cholangiocarcinoma: A systematic review and meta-analysis. *J Hepatol* (2020) 72(1):95–103. doi: 10.1016/j.jhep.2019.09.007
- Rizvi S, Khan SA, Hallemeier CL, Kelley RK, Gores GJ. Cholangiocarcinoma - evolving concepts and therapeutic strategies. *Nat Rev Clin Oncol* (2018) 15(2):95–111. doi: 10.1038/nrclinonc.2017.157
- Valle J, Wasan H, Palmer DH, Cunningham D, Anthony A, Maraveyas A, et al. Cisplatin plus gemcitabine versus gemcitabine for biliary tract cancer. *N Engl J Med* (2010) 362(14):1273–81. doi: 10.1056/NEJMoa0908721
- Liu M, Yang J, Xu B, Zhang X. Tumor metastasis: Mechanistic insights and therapeutic interventions. *MedComm* (2020) 2(4):587–617. doi: 10.1002/mco2.100
- Chen KK, Kovarikova A. Pharmacology and toxicology of toad venom. *J Pharm Sci* (1967) 56(12):1535–41. doi: 10.1002/jps.2600561202
- Li J, Ma X, Li F, Wang J, Chen H, Wang G, et al. Preparative separation and purification of bufadienolides from Chinese traditional medicine of ChanSu using high-speed counter-current chromatography. *J Sep Sci* (2010) 33(9):1325–30. doi: 10.1002/jssc.200900782
- Emam H, Zhao QL, Furusawa Y, Refaat A, Ahmed K, Kadowaki M, et al. Apoptotic cell death by the novel natural compound, cinobufotalin. *Chem Biol Interact* (2012) 199(3):154–60. doi: 10.1016/j.cbi.2012.07.005
- Han Y, Ma R, Cao G, Liu H, He L, Tang L, et al. Combined treatment of cinobufotalin and gefitinib exhibits potent efficacy against lung cancer. *Evid Based Complement Alternat Med* (2021) 2021:6612365. doi: 10.1155/2021/6612365
- Liu Y, Jiang Q, Liu X, Lin X, Tang Z, Liu C, et al. Cinobufotalin powerfully reversed EBV-miR-BART22-induced cisplatin resistance via stimulating MAP2K4 to antagonize non-muscle myosin heavy chain IIA/glycogen synthase 3beta/beta-catenin signaling pathway. *EBioMedicine* (2019) 48:386–404. doi: 10.1016/j.ebiom.2019.08.040
- Li LL, Su YX, Mao Y, Jiang PY, Chu XL, Xue P, et al. The effectiveness and safety of cinobufotalin injection as an adjunctive treatment for lung cancer: A meta-analysis of randomized controlled trials. *Evid Based Complement Alternat Med* (2021) 2021:8852261. doi: 10.1155/2021/8852261
- Zhang X, Liu T, Zhang Y, Liu F, Li H, Fang D, et al. Elucidation of the differences in cinobufotalin's pharmacokinetics between normal and diethylnitrosamine-injured rats: The role of p-glycoprotein. *Front Pharmacol* (2019) 10:521. doi: 10.3389/fphar.2019.00521
- Mao Y, Peng X, Xue P, Lu D, Li L, Zhu S. Network pharmacology study on the pharmacological mechanism of cinobufotalin injection against lung cancer. *Evid Based Complement Alternat Med* (2020) 2020:1246742. doi: 10.1155/2020/1246742
- Guo N, Miao Y, Sun M. Transcatheter hepatic arterial chemoembolization plus cinobufotalin injection adjuvant therapy for advanced hepatocellular carcinoma: a meta-analysis of 27 trials involving 2,079 patients. *Onco Targets Ther* (2018) 11:8835–53. doi: 10.2147/OTT.S182840
- Wang Z, Ma J, Miyoshi C, Li Y, Sato M, Ogawa Y, et al. Quantitative phosphoproteomic analysis of the molecular substrates of sleep need. *Nature* (2018) 558(7710):435–9. doi: 10.1038/s41586-018-0218-8
- Huang da W, Sherman BT, Lempicki RA. Systematic and integrative analysis of large gene lists using DAVID bioinformatics resources. *Nat Protoc* (2009) 4(1):44–57. doi: 10.1038/nprot.2008.211
- Sherman BT, Hao M, Qiu J, Jiao X, Baseler MW, Lane HC, et al. DAVID: a web server for functional enrichment analysis and functional annotation of gene lists (2021 update). *Nucleic Acids Res* (2022) 50(W1):W216–21. doi: 10.1093/nar/gkac194
- Zhou Y, Zhou B, Pache L, Chang M, Khodabakhshi AH, Tanaseichuk O, et al. Metascape provides a biologist-oriented resource for the analysis of systems-level datasets. *Nat Commun* (2019) 10(1):1523. doi: 10.1038/s41467-019-09234-6
- Licata L, Lo Surdo P, Iannuccelli M, Palma A, Micarelli E, Perfetto L, et al. SIGNOR 2.0, the SIGNaling network open resource 2.0: 2019 update. *Nucleic Acids Res* (2020) 48(D1):D504–D10. doi: 10.1093/nar/gkz949
- Zhou X, Zhou W, Liu W, Luo M, Wu X, Wang Y, et al. A network pharmacology approach to explore the mechanism of HuangZhi YiShen capsule for treatment of diabetic kidney disease. *J Trans Internal Med* (2021) 9(2):98–113. doi: 10.2478/jtjm-2021-0020
- Xu D, Liu L, Zhao Y, Yang L, Cheng J, Hua R, et al. Melatonin protects mouse testes from palmitic acid-induced lipotoxicity by attenuating oxidative stress and DNA damage in a SIRT1-dependent manner. *J Pineal Res* (2020) 69(4):e12690. doi: 10.1111/jpi.12690
- Yang F, Liao J, Yu W, Qiao N, Guo J, Han Q, et al. Exposure to copper induces mitochondria-mediated apoptosis by inhibiting mitophagy and the PINK1/parkin pathway in chicken (*Gallus gallus*) livers. *J Hazard Mater* (2021) 408:124888. doi: 10.1016/j.jhazmat.2020.124888
- von Karstedt S, Montinaro A, Walczak H. Exploring the TRAILS less travelled: TRAIL in cancer biology and therapy. *Nat Rev Cancer* (2017) 17(6):352–66. doi: 10.1038/nrc.2017.28
- Sheridan JP, Marsters SA, Pitti RM, Gurney A, Skubatch M, Baldwin D, et al. Control of TRAIL-induced apoptosis by a family of signaling and decoy receptors. *Science* (1997) 277(5327):818–21. doi: 10.1126/science.277.5327.818
- Hwang-Bo H, Lee WS, Nagappan A, Kim HJ, Panchanathan R, Park C, et al. Morin enhances auranofin anticancer activity by up-regulation of DR4 and DR5 and modulation of bcl-2 through reactive oxygen species generation in Hep3B human hepatocellular carcinoma cells. *Phytother Res* (2019) 33(5):1384–93. doi: 10.1002/ptr.6329
- Wu GS, Burns TF, McDonald ER3rd, Jiang W, Meng R, Krantz ID, et al. KILLER/DR5 is a DNA damage-inducible p53-regulated death receptor gene. *Nat Genet* (1997) 17(2):141–3. doi: 10.1038/ng1097-141
- Sharma K, D'Souza RC, Tyanova S, Schaab C, Wisniewski JR, Cox J, et al. Ultradeep human phosphoproteome reveals a distinct regulatory nature of tyr and Ser/Thr-based signaling. *Cell Rep* (2014) 8(5):1583–94. doi: 10.1016/j.celrep.2014.07.036
- Sacco F, Seelig A, Humphrey SJ, Krahmer N, Volta F, Reggio A, et al. Phosphoproteomics reveals the GSK3-PDX1 axis as a key pathogenic signaling node in diabetic islets. *Cell Metab* (2019) 29(6):1422–32 e3. doi: 10.1016/j.cmet.2019.02.012
- Yuan Z, Zhang X, Sengupta N, Lane WS, Seto E. SIRT1 regulates the function of the nijmegen breakage syndrome protein. *Mol Cell* (2007) 27(1):149–62. doi: 10.1016/j.molcel.2007.05.029
- Wu X, Ranganathan V, Weisman DS, Heine WF, Ciccone DN, O'Neill TB, et al. ATM Phosphorylation of nijmegen breakage syndrome protein is required in a DNA damage response. *Nature* (2000) 405(6785):477–82. doi: 10.1038/35013089
- Matsuoka S, Ballif BA, Smogorzewska A, McDonald ER3rd, Hurov KE, Luo J, et al. ATM and ATR substrate analysis reveals extensive protein networks responsive to DNA damage. *Science* (2007) 316(5828):1160–6. doi: 10.1126/science.1140321
- Gupta S, Seth A, Davis RJ. Transactivation of gene expression by myc is inhibited by mutation at the phosphorylation sites thr-58 and ser-62. *Proc Natl Acad Sci U.S.A.* (1993) 90(8):3216–20. doi: 10.1073/pnas.90.8.3216
- Hornbeck PV, Zhang B, Murray B, Kornhauser JM, Latham V, Skrzypek E. PhosphoSitePlus, 2014: mutations, PTMs and recalibrations. *Nucleic Acids Res* (2015) 43(Database issue):D512–20. doi: 10.1093/nar/gku1267
- Wiredja DD, Koyuturk M, Chance MR. The KSEA app: a web-based tool for kinase activity inference from quantitative phosphoproteomics. *Bioinformatics* (2017) 33(21):3489–91. doi: 10.1093/bioinformatics/btx415
- Sacco F, Silvestri A, Posca D, Pirro S, Gherardini PF, Castagnoli L, et al. Deep proteomics of breast cancer cells reveals that metformin rewires signaling networks away from a pro-growth state. *Cell Syst* (2016) 2(3):159–71. doi: 10.1016/j.cels.2016.02.005
- Wang Z, Gong Y, Peng B, Shi R, Fan D, Zhao H, et al. MRE11 UFMylation promotes ATM activation. *Nucleic Acids Res* (2019) 47(8):4124–35. doi: 10.1093/nar/gkz110
- Guo Z, Kozlov S, Lavin MF, Person MD, Paull TT. ATM Activation by oxidative stress. *Science* (2010) 330(6003):517–21. doi: 10.1126/science.1192912
- Smith HL, Southgate H, Tweddle DA, Curtin NJ. DNA Damage checkpoint kinases in cancer. *Expert Rev Mol Med* (2020) 22:e2. doi: 10.1017/erm.2020.3

43. Ou YH, Chung PH, Sun TP, Shieh SY. p53 c-terminal phosphorylation by CHK1 and CHK2 participates in the regulation of DNA-damage-induced c-terminal acetylation. *Mol Biol Cell* (2005) 16(4):1684–95. doi: 10.1091/mbc.e04-08-0689
44. Wang M, Chen S, Ao D. Targeting DNA repair pathway in cancer: Mechanisms and clinical application. *MedComm (2020)* (2021) 2(4):654–91. doi: 10.1002/mco2.103
45. Song C, Shi D, Chang K, Li X, Dong Q, Ma X, et al. Sodium fluoride activates the extrinsic apoptosis via regulating NOX4/ROS-mediated p53/DR5 signaling pathway in lung cells both *in vitro* and *in vivo*. *Free Radic Biol Med* (2021) 169:137–48. doi: 10.1016/j.freeradbiomed.2021.04.007
46. Sheikh MS, Fornace AJ Jr. Death and decoy receptors and p53-mediated apoptosis. *Leukemia* (2000) 14(8):1509–13. doi: 10.1038/sj.leu.2401865
47. Zhou X, Zijlstra SN, Soto-Gamez A, Setroikromo R, Quax WJ. Artemisinin derivatives stimulate DR5-specific TRAIL-induced apoptosis by regulating wildtype P53. *Cancers (Basel)* (2020) 12(9):2514. doi: 10.3390/cancers12092514
48. Kretz AL, Trauzold A, Hillenbrand A, Knippschild U, Henne-Bruns D, von Karstedt S, et al. TRAILblazing strategies for cancer treatment. *Cancers (Basel)* (2019) 11(4):456. doi: 10.3390/cancers11040456
49. Lee CF, Yang JS, Tsai FJ, Chiang NN, Lu CC, Huang YS, et al. Kaempferol induces ATM/p53-mediated death receptor and mitochondrial apoptosis in human umbilical vein endothelial cells. *Int J Oncol* (2016) 48(5):2007–14. doi: 10.3892/ijo.2016.3420
50. Guo X, Li K, Jiang W, Hu Y, Xiao W, Huang Y, et al. RNA Demethylase ALKBH5 prevents pancreatic cancer progression by posttranscriptional activation of PER1 in an m6A-YTHDF2-dependent manner. *Mol Cancer* (2020) 19(1):91. doi: 10.1186/s12943-020-01158-w
51. Banerjee D, Langberg K, Abbas S, Odermatt E, Yerramothu P, Volaric M, et al. A non-canonical, interferon-independent signaling activity of cGAMP triggers DNA damage response signaling. *Nat Commun* (2021) 12(1):6207. doi: 10.1038/s41467-021-26240-9
52. Jiang W, Tan Y, Peng Y. Aroyldihydrazone diorganotin complexes causes DNA damage and apoptotic cell death: From chemical synthesis to biochemical effects. *Int J Mol Sci* (2021) 22(24):13525. doi: 10.3390/ijms222413525
53. Sui X, Zhang C, Zhou J, Cao S, Xu C, Tang F, et al. Resveratrol inhibits extranodal NK/T cell lymphoma through activation of DNA damage response pathway. *J Exp Clin Cancer Res* (2017) 36(1):133. doi: 10.1186/s13046-017-0601-6
54. Yu Q, Pu SY, Wu H, Chen XQ, Jiang JJ, Gu KS, et al. TICRR contributes to tumorigenesis through accelerating DNA replication in cancers. *Front Oncol* (2019) 9:516. doi: 10.3389/fonc.2019.00516
55. Ji J, Chen W, Lian W, Chen R, Yang J, Zhang Q, et al. (S)-crizotinib reduces gastric cancer growth through oxidative DNA damage and triggers pro-survival akt signal. *Cell Death Dis* (2018) 9(6):660. doi: 10.1038/s41419-018-0667-x
56. Li Y, Liu X, Lin X, Zhao M, Xiao Y, Liu C, et al. Chemical compound cinobufotalin potently induces FOXO1-stimulated cisplatin sensitivity by antagonizing its binding partner MYH9. *Signal Transduct Target Ther* (2019) 4:48. doi: 10.1038/s41392-019-0084-3
57. McPherson MT, Holub AS, Husbands AY, Petreaca RC. Mutation spectra of the MRN (MRE11, RAD50, NBS1/NBN) break sensor in cancer cells. *Cancers (Basel)* (2020) 12(12):3794. doi: 10.3390/cancers12123794
58. Bian L, Meng Y, Zhang M, Li D. MRE11-RAD50-NBS1 complex alterations and DNA damage response: implications for cancer treatment. *Mol Cancer* (2019) 18(1):169. doi: 10.1186/s12943-019-1100-5
59. Zhao S, Renthal W, Lee EY. Functional analysis of FHA and BRCT domains of NBS1 in chromatin association and DNA damage responses. *Nucleic Acids Res* (2002) 30(22):4815–22. doi: 10.1093/nar/gkf612
60. Liang Z, Liu Z, Cheng C, Wang H, Deng X, Liu J, et al. VPS33B interacts with NESG1 to modulate EGFR/PI3K/AKT/c-Myc/P53/miR-133a-3p signaling and induce 5-fluorouracil sensitivity in nasopharyngeal carcinoma. *Cell Death Dis* (2019) 10(4):305. doi: 10.1038/s41419-019-1457-9
61. Cianfanelli V, Fuoco C, Lorente M, Salazar M, Quondamatteo F, Gherardini PF, et al. AMBRA1 links autophagy to cell proliferation and tumorigenesis by promoting c-myc dephosphorylation and degradation. *Nat Cell Biol* (2015) 17(1):20–30. doi: 10.1038/ncb3072
62. Zou LH, Shang ZF, Tan W, Liu XD, Xu QZ, Song M, et al. TNKS1BP1 functions in DNA double-strand break repair through facilitating DNA-PKcs autophosphorylation dependent on PARP-1. *Oncotarget* (2015) 6(9):7011–22. doi: 10.18632/oncotarget.3137
63. Qian H, Zhang Y, Wu B, Wu S, You S, Zhang N, et al. Structure and function of HECT E3 ubiquitin ligases and their role in oxidative stress. *J Trans Internal Med* (2020) 8(2):71–9. doi: 10.2478/jtim-2020-0012
64. Inagaki A, van Cappellen WA, van der Laan R, Houtsmuller AB, Hoeijmakers JH, Grootegoed JA, et al. Dynamic localization of human RAD18 during the cell cycle and a functional connection with DNA double-strand break repair. *DNA Repair (Amst)* (2009) 8(2):190–201. doi: 10.1016/j.dnarep.2008.10.008
65. Ko JH, Son MY, Zhou Q, Molnarova L, Song L, Mlcouskova J, et al. TREX2 exonuclease causes spontaneous mutations and stress-induced replication fork defects in cells expressing RAD51(K133A). *Cell Rep* (2020) 33(12):108543. doi: 10.1016/j.celrep.2020.108543
66. Kobayashi S, Kasaishi Y, Nakada S, Takagi T, Era S, Motegi A, et al. Rad18 and Rnf8 facilitate homologous recombination by two distinct mechanisms, promoting Rad51 focus formation and suppressing the toxic effect of nonhomologous end joining. *Oncogene* (2015) 34(33):4403–11. doi: 10.1038/onc.2014.371